Mutant ataxin1 disrupts cerebellar development in spinocerebellar ataxia type 1

Chandrakanth Reddy Edamakanti,[1] Jeehaeh Do,[2] Alessandro Didonna,[3] Marco Martina,[2] and Puneet Opal[1,4]

[1]Davee Department of Neurology, and [2]Department of Physiology, Feinberg School of Medicine, Northwestern University, Chicago, Illinois, USA. [3]Department of Neurology, UCSF, San Francisco, California, USA. [4]Department of Cell and Molecular Biology, Feinberg School of Medicine, Northwestern University, Chicago, Illinois, USA.

Spinocerebellar ataxia type 1 (SCA1) is an adult-onset neurodegenerative disease caused by a polyglutamine expansion in the protein ATXN1, which is involved in transcriptional regulation. Although symptoms appear relatively late in life, primarily from cerebellar dysfunction, pathogenesis begins early, with transcriptional changes detectable as early as a week after birth in SCA1-knockin mice. Given the importance of this postnatal period for cerebellar development, we asked whether this region might be developmentally altered by mutant ATXN1. We found that expanded ATXN1 stimulates the proliferation of postnatal cerebellar stem cells in SCA1 mice. These hyperproliferating stem cells tended to differentiate into GABAergic inhibitory interneurons rather than astrocytes; this significantly increased the GABAergic inhibitory interneuron synaptic connections, disrupting cerebellar Purkinje cell function in a non–cell autonomous manner. We confirmed the increased basket cell–Purkinje cell connectivity in human SCA1 patients. Mutant ATXN1 thus alters the neural circuitry of the developing cerebellum, setting the stage for the later vulnerability of Purkinje cells to SCA1. We propose that other late-onset degenerative diseases may also be rooted in subtle developmental derailments.

Introduction

Spinocerebellar ataxia type 1 (SCA1) is a paradigmatic polyglutamine disease: a CAG trinucleotide repeat tract undergoes expansion during DNA replication, which leads to an abnormally long polyglutamine tract in the encoded protein (in this case, ATXN1) that causes the protein to misfold and resist clearance (1–3). Like other polyglutamine proteins, ATXN1 is expressed throughout the brain, but tends to cause focal damage. In the case of SCA1, the site of greatest damage, and the source of the clinical presentation of ataxia, is the cerebellum (4, 5). It is not known why so many polyglutamine diseases (especially other SCAs) affect the cerebellum, but it should be noted that other regions are ultimately affected as well, particularly the brain stem.

Studies in SCA1 mouse models, which recapitulate the human disease with an adult-onset progressive loss of motor coordination, have demonstrated that pathogenic events begin long before the clinical signs present themselves. In both knockin and transgenic models of SCA1, defects in Purkinje cell (PC) synaptic connectivity precede ataxia (6–8), and gene expression changes appear within the first few weeks of life (8–13). During this early period, neurogenesis is still taking place within a niche of postnatal stem cells in the cerebellar white matter, which led us to ask whether early neurodevelopment might go awry in ways that alter the neural circuitry of the cerebellum. In light of our recent discovery that adult hippocampal stem cells expressing mutant human ATXN1 proliferate poorly (14, 15), we hypothesized that the cerebellar stem cell population might also behave differently under the influence of expanded ATXN1. For example, altered neural stem cell behavior could affect the reservoir of neurons available to replace sick cells that begin to degenerate in later life.

The stem cell niche that develops from the cerebellar ventricular zone (VZ) is characterized by the expression of prominin-1 (also known as CD133), a membrane-spanning glycoprotein that defines a subset of stem cells in the brain and hematopoietic systems. These stem cells reside in the prospective white matter during the first 3 weeks of postnatal life and contribute to the development of basket cells (BCs) and stellate cells — interneurons that synapse onto PCs and sculpt PC topography and function via GABAergic inhibition (16–18). The BCs innervate the PC soma and proximal dendrites, while the stellate cells act on the more distal dendrites. The stem cells also generate all postnatally derived cerebellar astrocytes through the formation of CD15-expressing astrocytic precursors (17, 19).

Here, we report that mutant ATXN1 increases the proliferation of cerebellar stem cells in the early postnatal period and biases their differentiation toward a neuronal lineage and away from an astrocytic lineage. This results in a greater-than-normal number of inhibitory neurons that inhibit PC firing. Given that CNS maturation is a well-regulated process, our results suggest that the structural development of the cerebellum in SCA1 is abnormal and that the resulting neural circuit is more vulnerable to the effects of mutant ATXN1.

Results

Increased proliferation of postnatal cerebellar stem cells in Sca1$^{154Q/2Q}$ knockin mice. To understand the pathogenesis of SCA1, we focused our investigation on SCA1-knockin mice (*Sca1*$^{154Q/2Q}$), which have 1 allele carrying a pathogenic polyglutamine stretch of 154 repeats and 1 allele expressing normal mouse *Atxn1* with 2 repeats (normal human alleles range from 6 to 44 polyglutamine repeats) (3, 20,

Conflict of interest: The authors have declared that no conflict of interest exists.
Submitted: August 8, 2017; **Accepted:** March 6, 2018.
Reference information: *J Clin Invest*. 2018;128(6):2252–2265.
https://doi.org/10.1172/JCI96765.

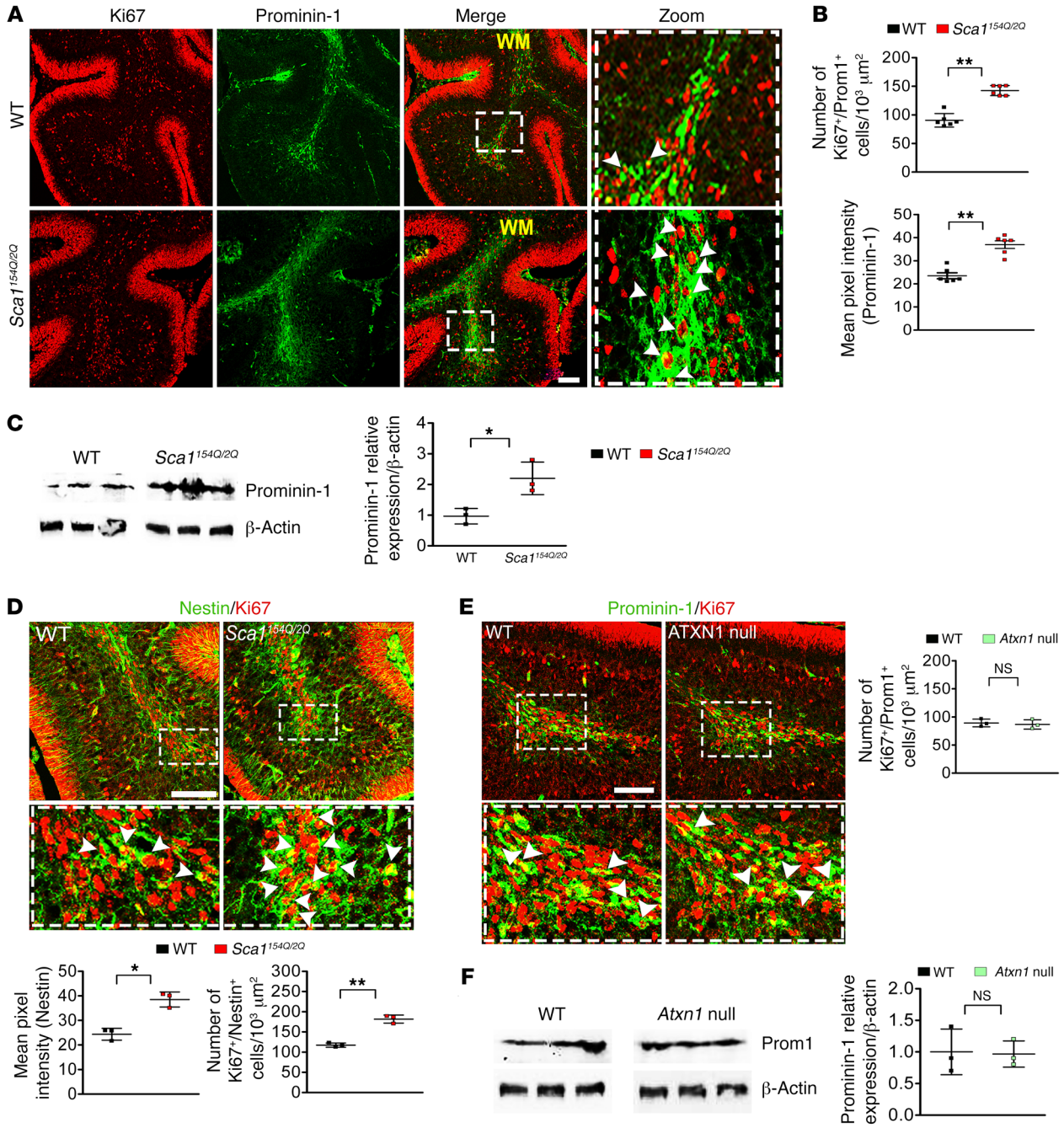

Figure 1. Mutant ATXN1 increases proliferation and enlarges the population of cerebellar stem cells at P7 in *Sca1*$^{154Q/2Q}$ mice. (**A**) Ki67 (red) and prominin-1 (green) staining show that SCA1 mice have greater cerebellar stem cell proliferation than WT controls at P7. Scale bar: 100 µm. *n* = 6 pairs of mice. (**B**) Quantification of prominin-1/Ki67 double-positive cells and intensity of prominin-1. (**C**) Western blot analysis and quantification show greater prominin-1 expression in SCA1 cerebella than in WT littermates. *n* = 3 independent mouse samples loaded in each lane for each genotype. See complete unedited blots in the Supplemental Figure 8. (**D**) We used Ki67 (red) and nestin (green) staining as an independent measure of cerebellar stem cell number and proliferation. Scale bar: 50 µm. *n* = 3 pairs of mice. (**E**) *Atxn1*$^{-/-}$ cerebellar sections costained with Ki67 (red) and prominin-1 (green) show numbers of double-positive cells similar to those in WT cerebella. Scale bar: 50 µm. *n* = 3 pairs of mice. Arrowheads indicate double-positive cells in A, D, and E. (**F**) Western blot analysis and quantification show that prominin-1 expression in *Atxn1*$^{-/-}$ cerebella is similar to that of WT cerebella. *n* = 3 independent mouse samples loaded in each lane for each genotype; lanes loaded onto same gel. See complete unedited blots in the Supplemental Figure 8. **P* < 0.05, ***P* < 0.01, 2-tailed unpaired Student's *t* test. Original magnification ×40 in **A**, **D**, and **E**.

21). These mice display the first signs of ataxia around 5 weeks of age (4, 8, 13) and exhibit alterations in PC synaptic connectivity around the same time (8). They exhibit gene-expression changes, however, as early as the first week of life (8, 9, 13).

In mice, stem cells expressing prominin-1, a stem cell marker, contribute to the development of GABAergic interneurons and astrocytes during the first 3 weeks of life (17, 18). To examine the number of cerebellar stem cells, we stained the cerebella of

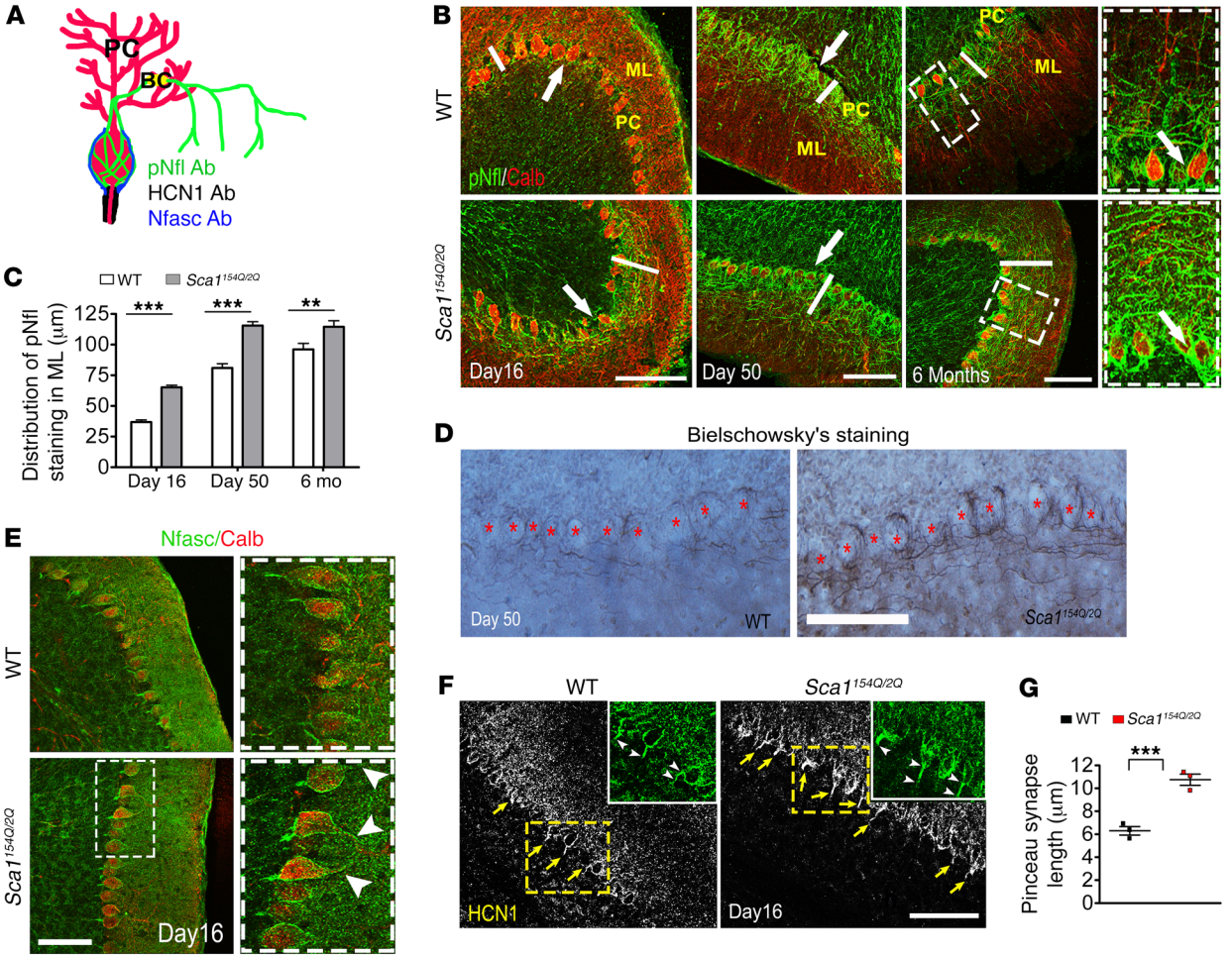

Figure 2. Exaggerated BC phenotype in *Sca1*$^{154Q/2Q}$ mice. (**A**) Schematic depicting BC (red) morphology with antibodies. Regions of BCs stained: pNfl (BC axonal and dendritic processes: green); HCN1 (Pinceau: black); Nfasc (PC somata and BC axonal ends: blue). (**B** and **C**) pNfl staining highlights profuse BC arborization around PCs (stained with calbindin) in the molecular layer of SCA1 cerebella at P16, P50, and 6 months of age. Arrows point to BC arbors surrounding PC soma; white bars mark the extent of BC collaterals extending into the molecular layer. n = 4 pairs of mice. (**D**) Representative images of Bielschowsky's silver–stained cerebella from SCA1 and WT mice. SCA1 mice show prominent BC axonal processes around PCs when compared with WT. Asterisks represent PC soma. (**E**) Nfasc staining (green) is intensified at the junction of BC axonal endings and PC soma (arrowheads). n = 3 pairs of mice. (**F**) HCN1 staining of cerebellar sections at P16 revealed that the SCA1 mice show exaggerated pinceau formation (arrows) compared with controls. (**G**) Quantification of the length of pinceau (distance between 2 arrowheads) using HCN1 staining. n = 3 pairs of mice. $^{**}P < 0.01$; $^{***}P < 0.001$, 2-tailed unpaired Student's t test. Scale bars: 100 μm. Original magnification ×40 in **B**, **E**, and **F**.

7-day-old *Sca1*$^{154Q/2Q}$ mice for prominin-1. The intensity of prominin-1 staining in the *Sca1*$^{154Q/2Q}$ cerebella was approximately 1.6 times greater than in cerebella from their WT littermate controls. We also stained for Ki67, a nuclear protein associated with cellular proliferation. Knockin mice had approximately 1.7 times as many double-positive cells as WT mice (Figure 1, A and B). Consistent with our immunohistochemical data, Western blot analysis revealed prominin-1 protein expression levels in cerebella from *Sca1*$^{154Q/2Q}$ mice to be approximately 2.5 times greater than those in WT mice (Figure 1C). As an independent measure, we also performed dual staining with Ki67 and nestin, a generic stem cell/neural progenitor cell marker, and obtained similar results for the number of double-positive cells and intensity of nestin staining in *Sca1*$^{154Q/2Q}$ cerebella (Figure 1D). Although SCA1 pathology is driven largely by a gain of function, i.e., enhanced interactions with a number of protein partners (22, 23), there is also some loss of ATXN1's normal function caused by diminished interactions with certain proteins (24, 25). To determine whether the enhanced proliferation is due to the loss of normal ATXN1 function, we tested the proliferative capacity of prominin-1–positive cerebellar stem cells from ATXN1-null mice (*Atxn1*$^{-/-}$) in vivo. There was no significant difference between the number of Ki67/prominin-1 double-positive cells in ATXN1-null and WT cerebella, as confirmed by Western blot analysis (Figure 1, E and F).

Cerebellar stem cells in Sca1$^{154Q/2Q}$ *mice tend to differentiate into GABAergic interneurons.* Given that postnatal cerebellar stem cells generate all the inhibitory GABAergic interneurons during cerebellar development (17, 19), we next explored whether the elevated stem cell proliferation in the developing cerebellum resulted in a concomitant increase in the number of these GABAergic interneurons. We stained postnatal cerebella with 2 different neuronal GABAergic precursor markers: Pax2, a transcription factor that

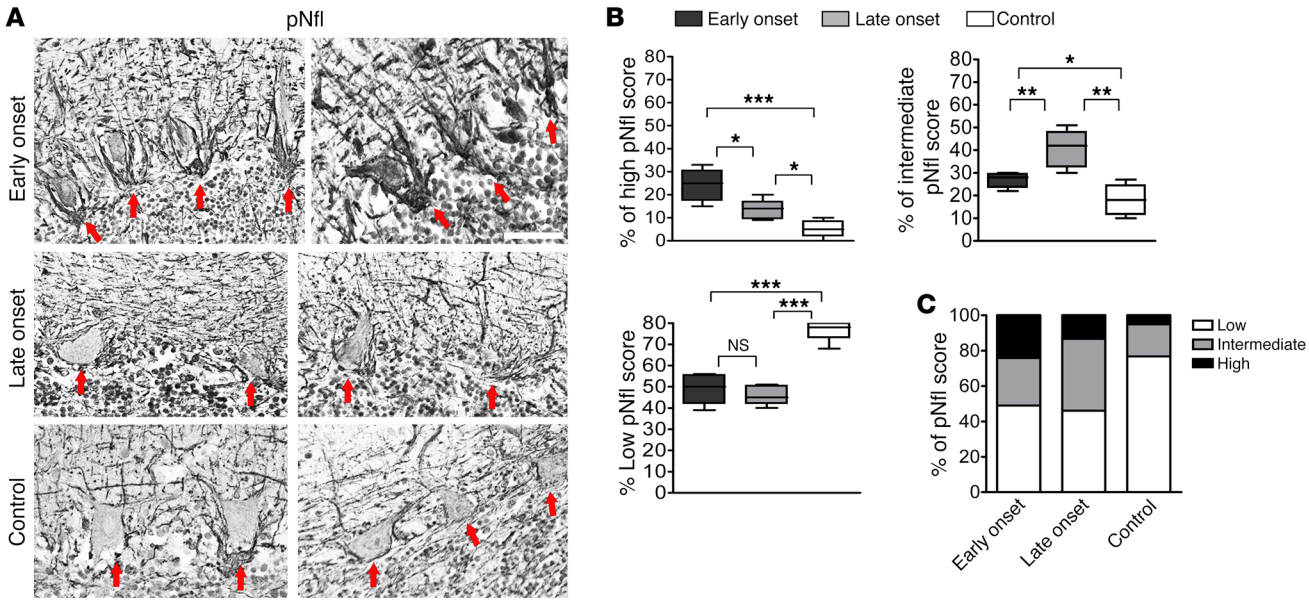

Figure 3. Brain tissue from human SCA1 patients with longer CAG repeat tracts shows denser BCs. (**A**) Representative images of cerebella from SCA1 patients and controls stained with pNfl. Photos are representative of 12 SCA1 patients; the samples come from patients with early onset and late-onset disease, as noted. Scale bar: 100 μM. (**B**) Quantification of pNfl score showing the percentage of low, intermediate, and high BC scores; 100 BCs/sample were counted. (**C**) Stacked bar graph shows the percentage of low, intermediate, and high BC scores of early onset, late-onset, and control cerebella. *$P < 0.05$; **$P < 0.01$; ***$P < 0.001$, 2-way ANOVA with Bonferroni's post hoc test.

defines GABAergic progenitors; and GAD67, an enzyme necessary for GABA synthesis that is expressed in both progenitors and matured GABAergic interneurons. There were approximately 1.6 times more Pax2-expressing cells in the *Sca1*$^{154Q/2Q}$ cerebella than in WT cerebella (Supplemental Figure 1, A and B; supplemental material available online with this article; https://doi.org/10.1172/JCI96765DS1) and a comparable increase in the intensity of GAD67 staining (~1.5-fold) (Supplemental Figure 1, C and D).

The GABAergic interneuron lineage gives rise to both BCs and stellate cells. Both cell types send inhibitory synaptic connections to Purkinje neurons, with BCs synapsing on PC somas and proximal dendrites and stellate cells synapsing on the more distal dendrites. Because the synaptic connections of BCs have been better characterized both from an electrophysiological and a morphological perspective, we focused our investigation on BCs (26–28).

BCs form complex arborizations with PCs. Axonal terminals from multiple BCs ensheathe PC somas at a ratio of 20–30:1, forming "baskets" that contain GABAergic chemical synapses (29). BCs also form ephaptic connections with PCs through the pinceau, a brush-shaped structure that is formed by a concentration of axonal terminals, with 5–7 BC axons at each axonal initial segment (AIS) of the PCs (Figure 2A). Pinceaux enable rapid ephaptic coupling of local electrical currents to influence the synchronization of PC firing (30).

The development of GABAergic innervation follows a strict time line starting at the second postnatal week and continuing into the fourth week (27). This highly regulated process involves multiple steps, from the initial migration of BCs into the PC layer to the first contact of BC axons onto Purkinje soma, the selective extension of the BC terminals toward the base of the flask-shaped PC soma, and the formation of complex arborization around the PC. To evaluate this process, we stained the cells with pNfl, an antibody specific to phosphorylated neurofilaments, which are cytoskeletal proteins that delineate the fine BC collaterals (26) (Figure 2A). SCA1 mice showed more pNfl-stained axonal processes extending into the molecular layer: 65 μm in *Sca*$^{154Q/2Q}$ versus 38 μm in WT at P16 ($P < 0.001$). This difference persisted into adulthood: 115 μm in SCA1 versus 75 μm in WT at P50 and 110 μm in SCA1 versus 90 μm in WT at 6 months (Figure 2, B and C). The greater number of BC axonal processes was confirmed by Bielschowsky silver staining (Figure 2D), a widely accepted technique to visualize neurite arborization, particularly in the cerebellum (31).

The extension of the BC axons toward Purkinje neurons is determined by a gradient of neurofascin (Nfasc), a cell-adhesion molecule expressed at contiguous surfaces of the BC axons and Purkinje soma (26, 27). Consistent with our observations with pNfl, we observed an upregulation of Nfasc as early as P16, the earliest time point tested, which persisted into adulthood (Figure 2E and Supplemental Figure 2). It is worth noting in this context that proteomic studies show Nfasc and GAD67 proteins to be elevated in SCA1-knockin mice (8).

To characterize pinceau morphology, we stained for hyperpolarization-activated cyclic nucleotide gated potassium channel 1 (HCN1) channels, which are localized at the presynaptic terminals of BCs at the pinceau (26, 32). We found that at P16, when BCs are still in the process of making connections with the AIS of PCs, SCA1 pinceaux are approximately 40% longer (~11 μm) than WT (~6 μm) ($P < 0.001$; Figure 2, F and G). This suggests that the number of BCs that converge onto the pinceaux is greater in *Sca1*$^{154Q/2Q}$ mice than in WT. SCA1 mice thus display a greater number of BCs and increased connectivity between BCs and PCs.

Human SCA1 brains display abnormally dense and tangled BC axonal processes. To determine whether these findings are relevant

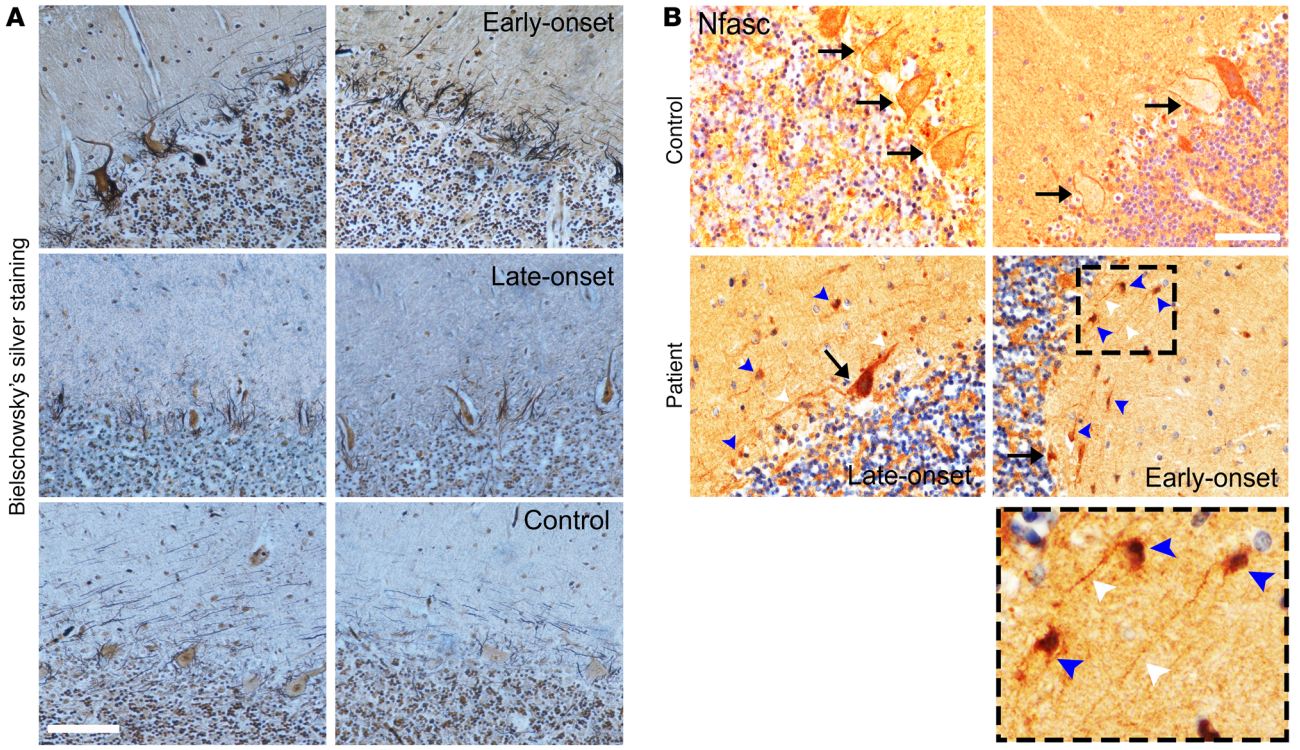

Figure 4. SCA1 patients show denser axonal processes and upregulated Nfasc expression in BCs. (**A**) Representative images of cerebellar tissue from SCA1 patients and controls stained with Bielschowsky's silver staining. Early onset patients show very dense BC axonal processes compared with late-onset patients, and control cerebella show sparse axonal processes around PCs. *n* = 2 samples from each category (early onset, late onset, and control). (**B**) Representative images of Nfasc-stained cerebella from SCA1 patients and controls. SCA1 patient cerebella show more intense Nfasc staining in both PCs (arrows) and BCs (arrowheads) than those of controls, with the more severe mutations producing greater changes. Scale bars: 100 μm. *n* = 12 patients and 7 controls. Original magnification ×40 in **B**.

to human SCA1, we examined BC morphology in postmortem tissue samples from SCA1 patients (*n* = 12 SCA1 patients, 7 controls; see Supplemental Table 1). Once again, we used pNfl and Bielschowsky's silver staining to delineate the fine BC axonal collateral densities around Purkinje soma. We also performed Nfasc staining to assess the expression levels of this adhesion molecule involved in axon guidance for correct BC-PC synapsing. BC axonal processes surrounding each PC soma were traced and quantified as described in Methods (100 PCs/brain) (31).

SCA1 patient tissues showed more profuse arborization of BC axons (Figure 3, A–C, pNfl staining; Figure 4A, Bielschowsky's stain). The extent of the increase in arborization was proportional to CAG repeat length (which governs the SCA1 phenotype, with more repeats producing more severe disease and earlier onset) (33–35, 36). In other words, the patients who showed earlier disease onset had more BC collaterals than those patients with milder, later-onset disease in the fifth or sixth decade of life (Figure 3, B and C). Similarly, tissues from early onset patients showed greater upregulation of Nfasc in PCs and BCs than either the tissues of late-onset patients or control tissues (Figure 4B). BC morphology in human SCA1 patient tissues thus parallels our findings in SCA1 mice.

Gain of ATXN1 function contributes to abnormal stem cell phenotype. To determine whether we could recapitulate the increased proliferation and differentiation of cerebellar stem cells in vitro, we isolated prominin-1–positive stem cells from the cerebella of *Sca1*$^{154Q/2Q}$ and WT mice and established primary cultures (16, 37). These cells retained their stem cell behaviors in vitro, namely, the capacity to proliferate, self-renew, express stem cell markers prominin-1, nestin, and glial fibrillary acidic protein (GFAP) (Figure 5, A and B), and differentiate into both neuronal and glial lineages, as evidenced by the expression of β-III tubulin and GFAP, respectively (Supplemental Figure 3, A–C). We counted the number of neurospheres formed from the cerebella of *Sca1*$^{154Q/2Q}$ mice and their WT littermates and found that *Sca1*$^{154Q/2Q}$ stem cells generated a greater number of neurospheres (~290 spheres/5,000 cells) than WT stem cells (~200 spheres/5,000 cells) (Figure 5, A and C). We also assessed the proliferation capacity of the stem cells in vitro by performing a BrdU incorporation assay, in which actively dividing cells incorporate the thymidine analogue BrdU. In our experiments, BrdU uptake was much greater in *Sca1*$^{154Q/2Q}$ stem cells than in the WT cells ($P < 0.001$; Figure 5C). Importantly, cerebellar stem cells from the *Sca1*$^{154Q/2Q}$ line continued to demonstrate self-renewal capacity (over at least 8 passages). We also found that these stem cells, when differentiated, showed an increase in Pax2-positive interneurons (Figure 5, D and E). Both of these results are consistent with our experiments in vivo.

To determine whether the loss of normal ATXN1 function might contribute to the enhanced cerebellar stem cell proliferation and differentiation in SCA1-knockin mice, we tested the proliferative and differentiation capacity of prominin-1–positive cerebellar

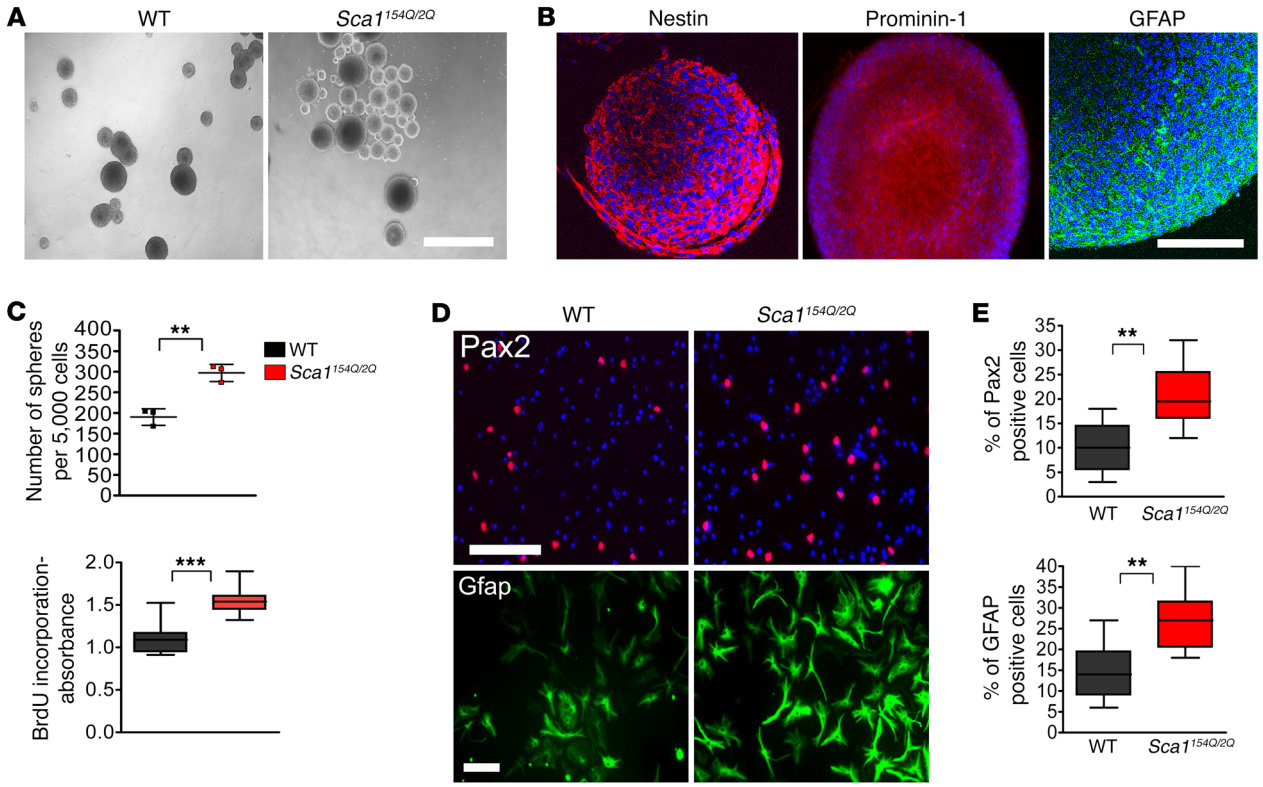

Figure 5. *Sca1*$^{154Q/2Q}$ cerebellar stem cells show increased proliferation and differentiation in vitro. (**A**) Neurospheres derived from isolated prominin-1$^+$ cerebellar stem cells of WT mice and SCA1 littermates. Scale bar: 100 μm. (**B**) Neurospheres express typical stem cell markers prominin-1, nestin, and GFAP. Scale bar: 50 μm. (**C**) The number of neurospheres derived from prominin-1–positive SCA1 cells is greater than that from WT controls; SCA1 cells also show greater BrdU uptake. n = 4 pairs of mice. (**D** and **E**) Differentiated cerebellar stem cells stained for GABAergic. Scale bars: 50 μm (Pax2); 100 μm (glial markers GFAP). SCA1 stem cells yield a greater number of both Pax2 and GFAP cells than WT stem cells. n = 3 pairs of mice. $^{**}P < 0.01$; $^{***}P < 0.001$, 2-tailed unpaired Student's t test.

stem cells isolated from ATXN1-null mice (*Atxn1*$^{-/-}$). We observed no change in the number of neurospheres or Pax2 cells from stem cells derived from ATXN1-null mice compared with those derived from WT controls (Figure 6, A–D). The altered stem cell phenotype in the *Sca1*$^{154Q/2Q}$ mice thus seems to be caused by a gain of ATXN1 function within the cerebellar stem cells themselves.

We next took advantage of the transgenic mouse line *ATXN1[82Q]*, in which mutant ATXN1 is expressed in PCs under the PC-specific promoter Pcp-2 (38) to determine whether stem cell proliferation or the later increase in BC arborization might be influenced by signals emanating from PCs expressing mutant ATXN1. Stem cells from the *ATXN1[82Q]* line did not differ from those from WT mice in their ability to proliferate (Supplemental Figure 4A) or differentiate (Supplemental Figure 4B), and their BC arborization was similar to that of WT (Supplemental Figure 4C). These results suggest that both the stem cell and BC phenotypes observed in SCA1-knockin mice and human patients result from processes intrinsic to cerebellar stem cells and not because of indirect effects from dysfunctional PCs.

As a further test to mirror the proliferation and fate of cerebellar stem cells, we transduced cerebellar stem cells isolated from WT mice with lentiviral particles carrying unexpanded GFP-*ATXN1[2Q]*, mutant expanded GFP-*ATXN1[82Q]* and control GFP. We found that both constructs increased cerebellar stem cell proliferation. Moreover, stem cells expressing ATXN1[82Q] produced more neurospheres than cells expressing ATXN1[2Q] (Figure 7D). These in vitro findings demonstrate that mutant ATXN1 stimulates cerebellar stem cell proliferation. To our surprise, during the course of these lentiviral experiments, we discovered that ATXN1 overexpression drove stem cell differentiation toward the GABAergic lineage and away from the astrocytic lineage. The proportion of differentiating cells that were Pax2 positive was 60% (for ATXN1[2Q]) and 82% (for ATXN1[82Q]) compared with 25% of control cells expressing GFP (Figure 7, A and C). The GFAP-positive cells, on the other hand, formed only 5% and 3% of the 2Q and 82Q populations, respectively, compared with 20% of control cells expressing GFP (Figure 7, B and C). The insignificant difference between the 2Q and 82Q GFAP-expressing cells likely reflects the fact that strong overexpression of ATXN1 obscures the effect of repeat length. These data suggest that a cell-autonomous gain of function of ATXN1 could tilt the lineage away from glial to a GABAergic lineage.

To determine whether this loss in glial lineage takes place in the *Sca1*$^{154Q/2Q}$ cerebellum in vivo, we stained the cerebella with GFAP to mark Bergmann glia and astrocytes that reside in the granular layer (velate astrocytes). Surprisingly, there was significantly less GFAP staining in the granular layer of *Sca1*$^{154Q/2Q}$ cerebella than in control cerebella at both P18 and 5 months of age (Figure 8A), the

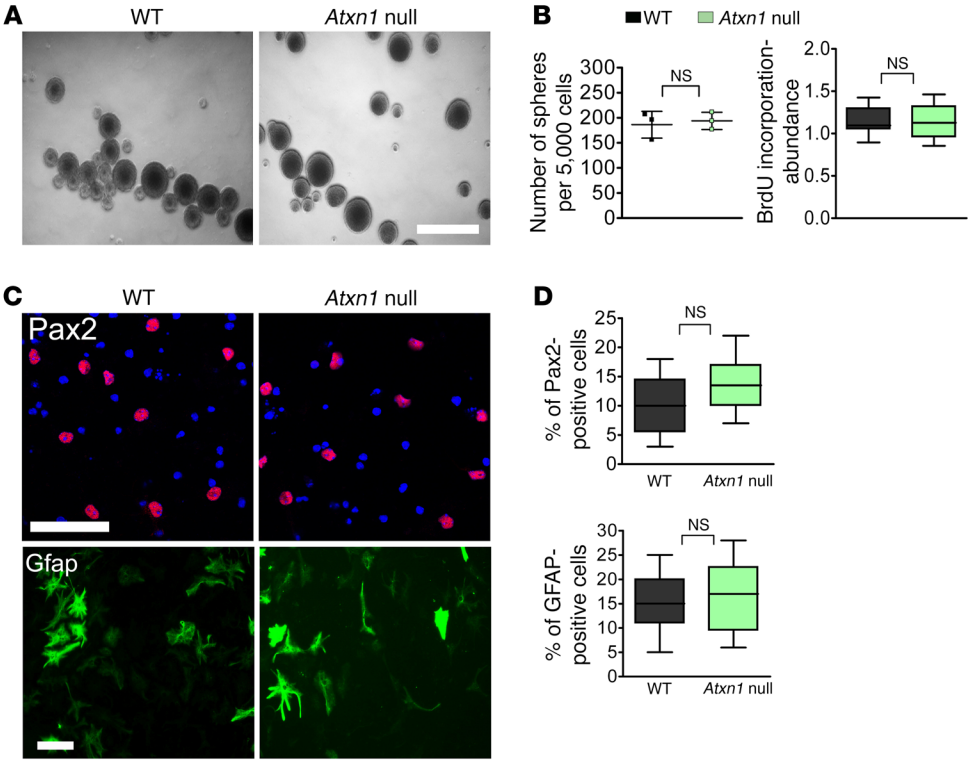

Figure 6. Gain of ATXN1 function contributes to the abnormal cerebellar stem cell phenotype. (**A** and **B**) Neurospheres derived from isolated prominin-1 stem cells of *Atxn1*$^{-/-}$ mice show proliferative capacity similar to that of WT stem cells. Scale bar: 100 μm. n = 3 pairs of mice. (**C** and **D**) Differentiated cerebellar stem cells stained for GABAergic. Scale bars: 50 μm (Pax2); 100 μm (glial markers GFAP). *Atxn1*$^{-/-}$ stem cells and WT stem cells resulted in a similar number of Pax2 and GFAP cells. n = 3 pairs of mice. Two-tailed unpaired Student's t test.

same time points at which we had observed exaggerated GABAergic BC innervation. These changes are distinct from the increased GFAP staining we observed in reactive Bergmann glia (Supplemental Figure 5, A and B) (39). Strikingly, the velate astrocytes isolated from *Sca1*$^{154Q/2Q}$ cerebella had lower proliferative capacity than astrocytes from controls (Supplemental Figure 6, A and B).

Approximately 10%–20% of BC axonal terminals cover the AIS at the pinceau; the majority are separated from PC AIS by astrocyte processes (40) (Figure 8B). This unique anatomic configuration of astrocytes at the pinceau is thought to play a crucial role in BC-induced ephaptic inhibition (40). To study the neuronal-glial interface, we costained the cerebellar sections with GFAP and calbindin. The number of connections between astrocytes and PCs in *Sca1*$^{154Q/2Q}$ mice was markedly lower than in WT controls (Figure 8C).

SCA1-knockin mice have more GABAergic synapses in the cerebellum, leading to an increased inhibition of PCs. Within the molecular layer, BCs are part of a circuit in which they are activated by granular cell parallel fibers to inhibit PC activity. To determine whether the overabundance of BCs in *Sca1*$^{154Q/2Q}$ mice results in a greater inhibition of PCs, we performed electrophysiological recordings to measure GABAergic interneuron-driven inhibitory postsynaptic currents (IPSCs) converging onto the PCs of SCA1 mice starting from the second week of age.

Previous studies in WT mice have already shown that inhibition of GABAergic interneurons is developmentally regulated: it is high in the first 2 weeks of postnatal life and then decreases between the third and fifth week, after which it stabilizes (41). In our electrophysiological experiments, we detected the same trend, but the frequencies and amplitudes of IPSCs were significantly higher in *Sca1*$^{154Q/2Q}$ PCs than those of control PCs at the age of P20–P24 (Figure 9, A and B).

We next measured the densities of inhibitory synaptic inputs onto PCs. We stained SCA1 and WT cerebella for the vesicular GABA transporter (vGAT), which marks GABAergic presynaptic terminals. Consistent with our functional measures, we found greater inhibitory synapse densities on PC soma of *Sca1*$^{154Q/2Q}$ cerebella (15 vGAT puncta/PC soma) than on those of WT controls (21 vGAT puncta/PC soma) (Figure 9, C and E). In parallel, we performed quantitative electron microscopy (EM) analysis of synaptic vesicle load in BC fibers (BFs). The average synaptic vesicle density of *Sca1*$^{154Q/2Q}$ BC fibers was greater than that of WT fibers (23 vs. 16 vesicles/bouton) (Figure 9, D and E). These results indicate that mutant BCs are characterized by increased GABAergic synapse strength and thus lead to strong inhibition of PCs.

Discussion

Neurodegenerative disorders typically manifest in mid-life or later. This is true not only for mostly sporadic syndromes such as Alzheimer's disease, Parkinson's disease, and amyotrophic lateral sclerosis, but also for the purely genetic polyglutamine neurodegenerative diseases, such as SCA1. This has led to an understandable emphasis on the role of aging in neurodegeneration. Yet it has been increasingly appreciated that pathogenic processes begin long before signs or symptoms develop at the organismal level; the current study sheds light on the earliest developmental anomalies yet to be described in SCA1.

Previous studies have observed that, by the end of the first postnatal month, SCA1 mice have synaptic abnormalities that involve alterations in climbing fiber (CF) glutamatergic input onto PCs (8, 9, 13). In this report, we demonstrate that the cerebellar network is altered in SCA1 even earlier than this through the involvement of cerebellar stem cells. These cells, identified just

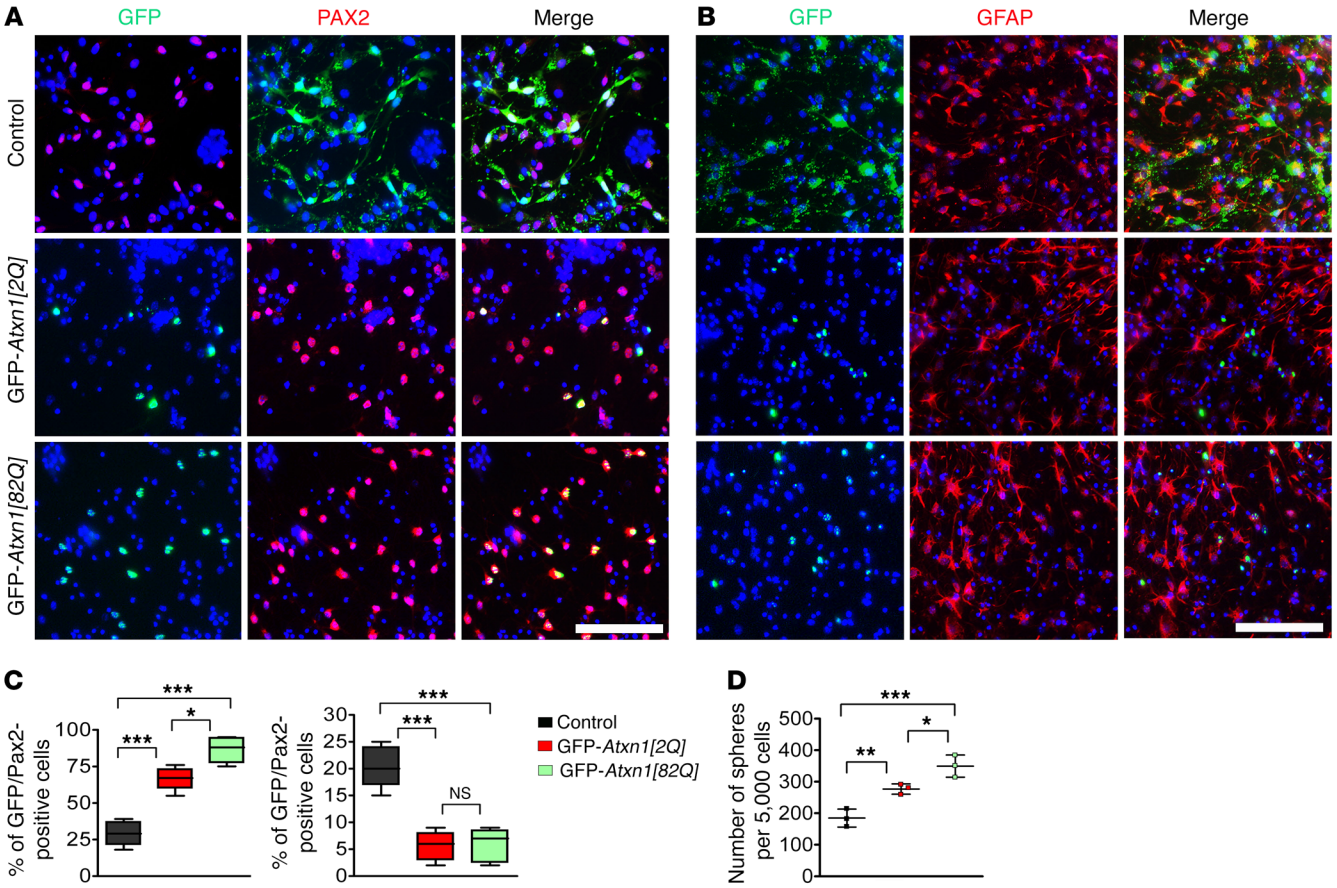

Figure 7. ATXN1 determines the GABAergic and glial lineage specificity of cerebellar stem cells. Differentiation of WT stem cells transduced with lentivirus particles expressing GFP, GFP-*ATXN1[2Q]*, and GFP-*ATXN1[82Q]* constructs. (**A**) Mutant ATXN1 produced significantly more GABAergic precursors (revealed by Pax2 staining) and (**B**) fewer glial precursors (revealed by GFAP staining). (**C**) Quantification of both Pax2/GFP- and GFAP/GFP-positive cells. $n = 3$ independent experiments. (**D**) Number of neurospheres formed from WT stem cells that are transduced with lentiviral vectors expressing GFP (control), GFP-*ATXN1[2Q]*, or GFP-*ATXN1[82Q]*. $n = 3$ pairs of mice. $^*P < 0.05$; $^{**}P < 0.01$; $^{***}P < 0.001$; 2-tailed unpaired Student's *t* test. Scale bars: 100 μm.

over a decade ago, have only recently been found to play a role in cerebellar development, and much less is known about them than the better-studied stem cells located in the VZ and the hippocampus. That expanded ATXN1 can modulate the proliferation and fate of these cells suggests that ATXN1 influences fundamental cell biological signaling events.

The period during which mutant ATXN1 promotes BC differentiation overlaps with the stage when definitive PC connections are formed. In the first weeks after birth, perisomatic innervation of PCs switches from excitatory glutamatergic CFs to inhibitory GABAergic BC fibers (BFs) (42). In SCA1, during the first 3 postnatal weeks, mutant ATXN1 exaggerates this switch by markedly increasing GABAergic BC inhibitory inputs (BF innervations). By 5 weeks of age, when the first symptoms manifest, SCA1 mice have fewer than normal glutamatergic inputs (CF innervations) onto PCs and attendant proteomic changes (8). The profound alterations in inhibitory and excitatory transmission over time may help explain the particular vulnerability of cerebellar PCs to SCA1 pathogenesis (Figure 10).

Altered BC connectivity has not been reported for any neurodegenerative ataxia, but it has been found in autopsy samples of patients suffering from essential tremor, another movement disorder that is cerebellar in origin (31, 43, 44). This, along with our observation that BC morphology correlates with CAG expansion and disease severity, supports the notion that this structural abnormality is truly pathogenic.

Given the augmented proliferation of cerebellar stem cells and the fact that our experiments measured populations of cell types relative to one another, it is still not clear whether the increase in the population of GABAergic interneurons occurs at the expense of the velate astrocyte population or reflects less proliferation of the astrocytic lineage after astrocytes are formed (Supplemental Figure 7). These are not mutually exclusive scenarios; indeed, our data provide support for both possibilities. Overexpression of ATXN1 using lentivirus (Figure 7) suggested that mutant ATXN1 exerts an influence reminiscent of Achaete-scute homolog 1 (Ascl-1), which draws the cerebellar stem cells toward the GABAergic lineage and away from the astrocyte lineage (45, 46). Culturing astrocytes from postnatal SCA1-knockin mice, on the other hand, demonstrated the low proliferative capacity of nascent astrocytes when they express expanded ATXN1 (Supplemental Figure 6). Resolving the relative contributions of each process to the diminished number of velate astrocytes will require fate-mapping analysis of cerebellar stem cells in SCA1 mice.

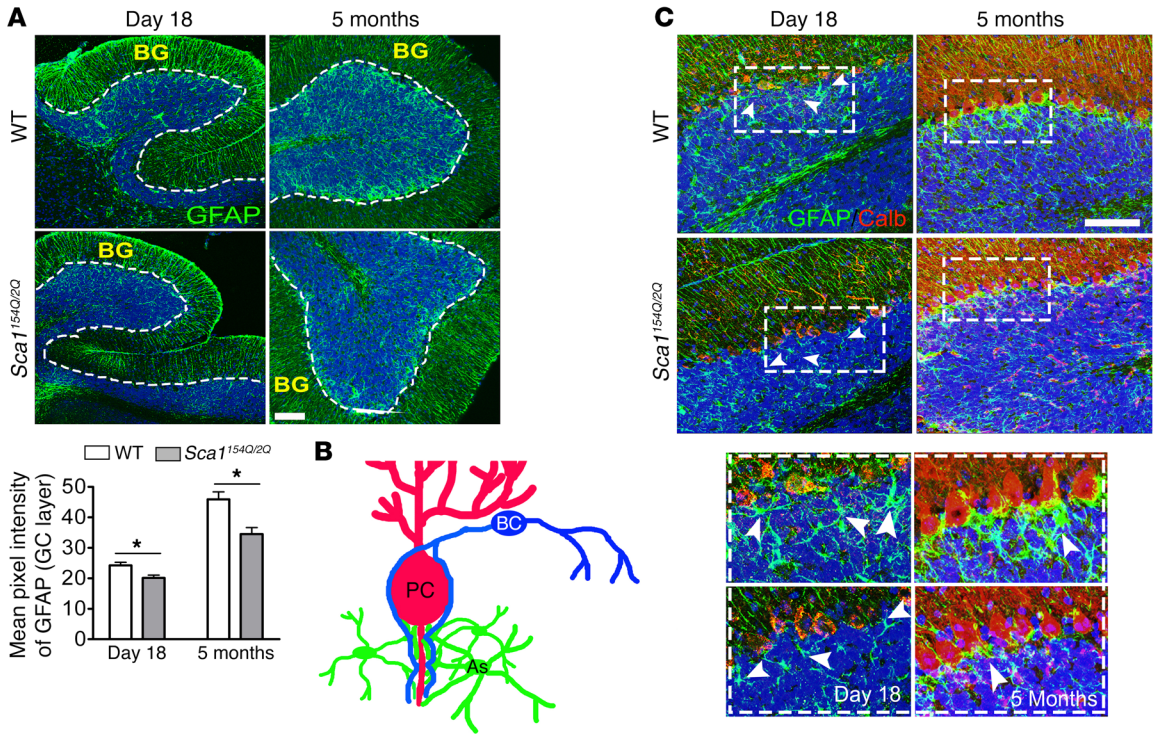

Figure 8. *Sca1*$^{154Q/2Q}$ mice cerebella show fewer white matter astrocytes than WT. (**A**) SCA1 cerebellum has less GFAP staining, indicating fewer velate astrocytes than WT cerebella, at P18 and 5 months. (**B**) Schematic showing that the majority of the PC AIS is covered by astrocyte (As) processes. (**C**) Costaining of cerebella (P18 and 5 months) with calbindin and GFAP shows the loss of connection between astrocytes and PC AIS (arrowheads). n = 3 pairs of mice. *$P < 0.05$, 2-tailed unpaired Student's t test. Scale bars: 100 μm. Original magnification ×40 in **B**.

In either case, this diminished astrocyte population is likely to stress the PCs in SCA1 by being inadequate to sustain the metabolic needs of surrounding neurons, regulate the release of neurotransmitters, or promote the reuptake of excessive neurotransmitters to protect the neurons from excitotoxicity. Indeed, several studies have shown that the ablation of astrocytes or the presence of abnormal astrocytes in the developing or adult cerebellum causes loss of PCs or cerebellar atrophy (47–49). A developmental decrease in velate astrocytes and high reactivity of Bergmann glial cells in SCA1 might also alter the inflammatory response (39, 50). We do not know why the Bergmann glial astrocytes and velate astrocytes adopt different fates in SCA1, but it is possible that these 2 populations are influenced by other signals. (For example, the Sonic Hedgehog pathway has been implicated in glial-neuronal decision points in the cerebellum; refs. 17, 51.)

It is still unclear how ATXN1 induces these proliferation and differentiation effects. A reasonable hypothesis is that ATXN1, a transcriptional repressor, changes the gene-expression signature of cerebellar stem cells and perhaps also that of their neuronal and glial progeny. More puzzling is why mutant ATXN1 would stimulate proliferation of cerebellar stem cells in early postnatal development when it suppresses proliferation of adult hippocampal stem cells (14). The explanation might lie in the different functions served by these distinct populations of stem cell: cerebellar stem cells populate the region with neurons and astrocytes during development (52), whereas adult hippocampal stem cell populations provide a reservoir for responding to environmental cues such as exercise or social isolation, which require adaptations in learning and memory (53). It will be important to investigate these questions experimentally and study other embryonic stem cell niches to determine whether the SCA1 brain undergoes other developmental aberrations. Regardless of the answers that may be specific to SCA1, this work raises the possibility that other adult-onset neurodegenerative conditions might have their roots in early developmental derangements. If this turns out to be the case, we will need to rethink our current models of pathogenesis and consider new strategies for therapy.

Methods

Mouse lines. The generation of *Atxn1*$^{-/-}$, *Sca1*$^{154Q/2Q}$, and *ATXN1[82Q]* mice has been described previously (4, 39, 54). The *Sca1*$^{154Q/2Q}$ line was generated by knocking 154 CAG repeats into the mouse locus with a small flanking region derived from a human sequence (but conserved in mice). The *Atxn1*$^{-/-}$ and *Sca1*$^{154Q/2Q}$ mice were originally generated on a C57BL/6J-129SvEv mixed background, but have been backcrossed more than 10 generations with C57BL/6J mice to eliminate possible confounding effects of mixed genetic background. The *ATXN1[82Q]* mice were generated and maintained on a pure FVB/N background.

Neurosphere cultures. Prominin-1–positive stem cells were isolated from mouse cerebella shortly after birth (P5–P7). Briefly, the meninges and choroid plexus were removed from the cerebella, which were then washed 3 times with ice-cold HBSS. A single-cell suspension was then prepared from each cerebellum using the Neuronal Tissue Dissociation Kit (Miltenyi Biotech; catalog 130-092-333). To select for stem cells expressing prominin-1, the cell suspension was incubated with anti–prominin-1 magnetic beads, immunopurified, and

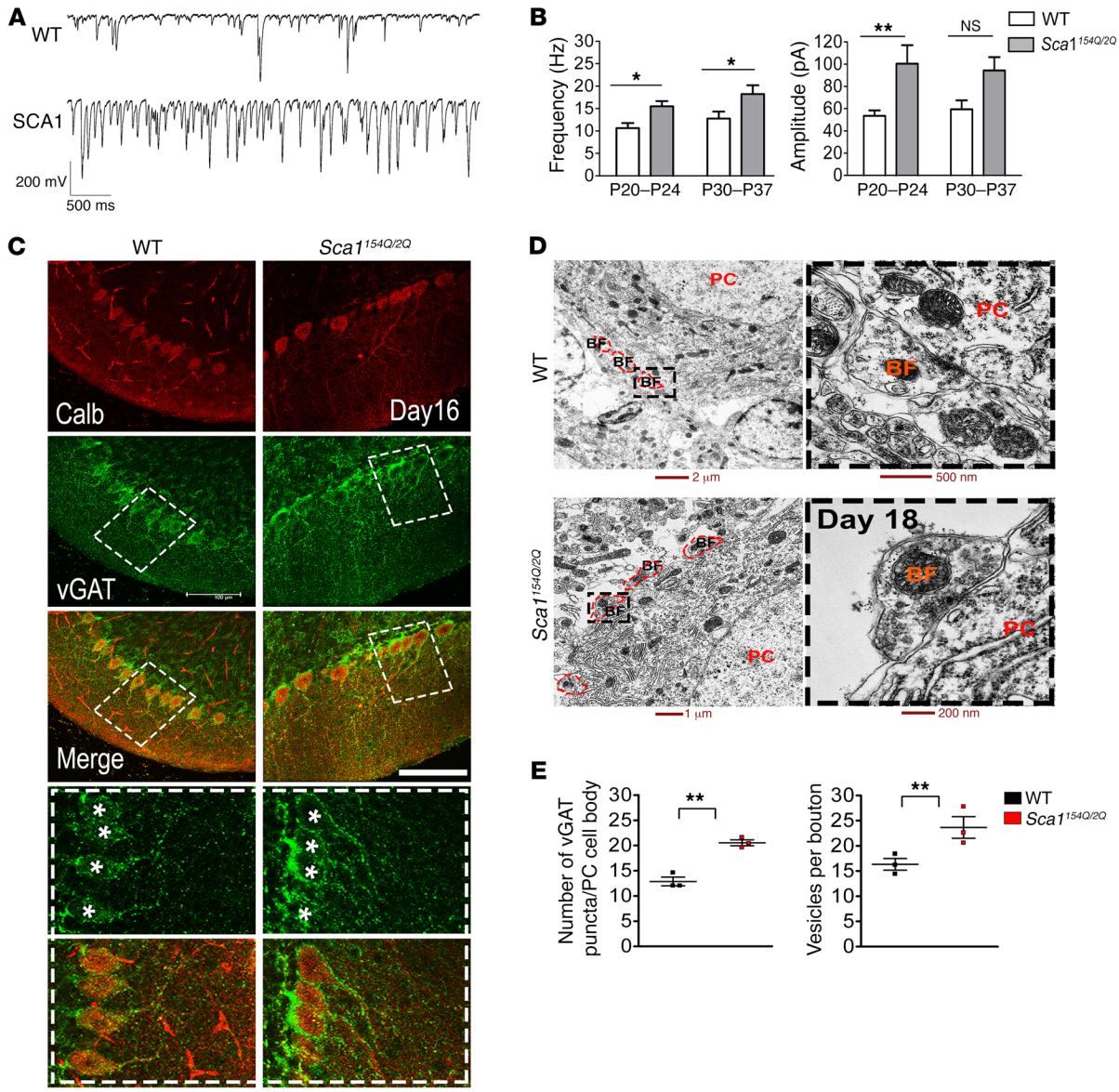

Figure 9. GABAergic inhibition of PCs is stronger in *Sca1*$^{154Q/2Q}$ mice. (**A** and **B**) IPSC frequencies and amplitudes are higher in SCA1-knockin mice than in WT controls. *n* = 4 pairs of mice. (**C**) vGAT (green), which marks GABA vesicles, and calbindin (red), which marks PCs, shows SCA1 mouse cerebella have more GABAergic presynaptic terminals than WT controls (asterisks represent PC soma). Scale bar: 100 μm. *n* = 3 pairs of mice. Original magnification ×40 in **C**. (**D**) EM images show SCA1 BC boutons have greater vesicle density than WT boutons. Scale bars: 500 and 200 nm (Enlarged images of the boxed areas) 2 μm and 1 μm for lower magnification images. *n* = 3 pairs of mice. (**E**) Quantification of GABAergic presynaptic terminals and GABA vesicles. $^*P < 0.05$; $^{**}P < 0.01$, 2-tailed unpaired Student's *t* test (**E**) and 2-way ANOVA with Bonferroni's post hoc test (**B**). Scale bar: 100 μm (**C**).

suspended in neurobasal medium containing penicillin/streptomycin with L-glutamine (Gibco; Thermo Fisher Scientific), 2% B27 (Gibco; Thermo Fisher Scientific), 20 ng/ml human recombinant EGF (Promega, catalog G502A), and 20 ng/ml human recombinant basic FGF (bFGF) (Promega, catalog G507A) and then plated in 24-well plates (at a density of 50,000 cells per well) to allow for the formation of neurospheres. To selectively enrich for neurospheres, the cells were plated onto low adhesive plates (Corning Ultra-Low attachment surface) that did not support the growth of neurons or glia. The neurospheres were cultured for 10 to 12 days; we refreshed the medium every 4 days. Secondary and tertiary neurospheres were made by passaging single cells from primary neurospheres using trypsinization (16). All experiments were performed on either secondary or tertiary neurospheres to obtain pure self-renewed stem cells; neurospheres were used for further neuronal differentiation.

For the neurosphere formation assay, the cells were plated in proliferation medium at a density of 5,000 cells per 24-well plate. The cells were then allowed to grow for 7 days, after which the number of neurospheres was evaluated using a light microscope (Zeiss). At least 4 mice for each genotype were used in independent assays.

Neurosphere differentiation. The neurospheres were pelleted by centrifugation at 300 *g* for 10 minutes and trypsinized to obtain a single-cell suspension. Dissociated cells were then cultured in neurobasal medium supplemented with 10 ng/ml differentiated factor

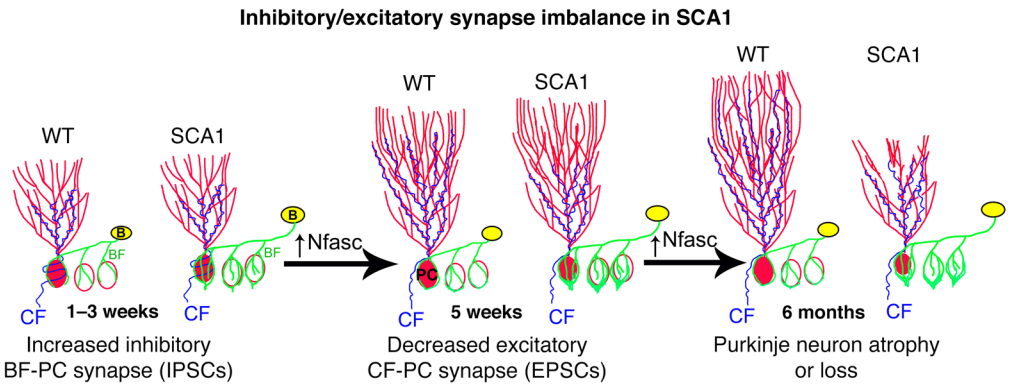

Figure 10. Model of the development of inhibitory/excitatory imbalance in SCA1 cerebellum. Increased GABAergic basket cell fibers innervations (green) from basket cells ('B'/yellow ovals) onto PCs occurs during the first 3 postnatal weeks in SCA1 mice, followed by an increase in IPSCs in PCs at P20–P24 (Figure 9). A decrease in glutamatergic CF synapses (blue) occurs at 5 weeks (and is manifested in motor incoordination on the rotarod), followed by PC atrophy or loss (red). B, basket cells.

PDGF-AA and 2% B2, without EGF and bFGF. After 7 days of in vitro (DIV7) growth, the cultures were fixed with 4% paraformaldehyde (PFA) for immunostaining or lysed with RIPA buffer (0.1% SDS, 0.5% sodium deoxy cholate, 1% Triton X-100, protease inhibitors, and 25 mM Tris HCl) or Laemmli buffer (4% SDS, 20% glycerol, 10% 2-mercaptoethanol, 0.004% bromophenol blue and 0.125 M Tris HCl) for Western blot analysis.

Immunoblotting assay. Neurospheres, differentiated cells, and cerebellar tissues were lysed on ice for 10 minutes in RIPA buffer containing protease inhibitors. Lysates were then cleared at 300 *g* for 30 minutes, and the supernatants were stored at –80°C until use. Total proteins were separated by SDS-PAGE (on 10% polyacrylamide gels) and transferred to nitrocellulose membranes (Amersham). The membranes were first blocked for 1 hour with 5% milk in 1× TBS-T (0.05% Tween-20) and then incubated with primary antibody (1:1000) overnight at 4°C. The next day, the membranes were washed and incubated with HRP-conjugated secondary antibodies (1:500) for 1 hour at room temperature (RT). After thorough washing in TBS-T, the nitrocellulose membranes were incubated with Super Signal West Pico Reagent (Thermo Scientific) and the chemiluminescent signals were detected using a Molecular Imager ChemiDoc XRS System equipped with Quantity One software (Bio-Rad) (55).

Cerebellar astrocyte cultures. Astrocytes were cultured based on published protocols with a few modifications (56). To obtain a sufficient number of astrocytes, 3 mice per genotype were pooled for each preparation. Mice were sacrificed at P4, and the cerebella were dissected from the choroid plexus and covering meninges, washed 3 times with ice-cold HBSS, and then incubated in 2.5% trypsin-EDTA solution (Gibco, Thermo Fisher Scientific; catalog 25200-056) at 37°C for 30 minutes, with intermittent shaking every 10 minutes. After a short centrifugation (5 minutes at 300 *g*) to remove the supernatant, trypsinized cerebella were dissociated by gently pipetting in astrocyte medium (DMEM, high glucose + 10% heat-inactivated fetal bovine serum + 1% penicillin/streptomycin) until a single-cell suspension was obtained. The cells were then seeded in poly-D-lysine–coated (PDL-coated) T25 flasks and incubated at 37°C, with the medium refreshed every 2 days. After 7 to 8 days, to increase the purity of the cultures, astrocytes were separated from less adherent cell types by differential shaking (30 minutes at 180 rpm to remove microglia and then 6 hours at 240 rpm to remove oligodendrocyte precursor cells). The remaining astrocytes were then reseeded in T25 flasks and grown for an additional 10 to 12 days, until confluence. These highly pure astrocyte preparations were used for all our experiments.

In vitro BrdU proliferation assay. To measure stem cell proliferation, we used a BrdU Cell Proliferation Assay Kit (Cell Signaling Technology). We plated 50,000 cerebellar stem cells per 96-well plate (low adherent to allow for neurosphere formation). The next day, BrdU solution was added to each well and the cells were incubated for another 24 hours. The cells were then fixed with 4% PFA and stained with primary BrdU antibody for 1 hour at RT. The signal was then developed using an HRP-conjugated secondary antibody and TMB substrate. The relative absorbance was measured at 450 nm using a dial-wavelength spectrophotometer (Spectramax).

Immunohistochemistry and Bielschowsky's silver staining. Mice were deeply anesthetized using isoflurane followed by transcardial perfusion with PBS followed by 4% PFA. The cerebella were then dissected and post-fixed with 4% PFA in PBS overnight at 4°C. They were subsequently equilibrated in 10%–30% sucrose gradient and embedded in OCT medium. The cerebella were then sliced into 30 μm–thick sections with a cryostat (Microm M505, Thermo Fisher Scientific) and processed for immunofluorescence.

For immunostaining, the sections were permeabilized and blocked with 10% normal goat serum and 0.25% Triton X-100 in 1× TBS (Tris-buffered saline) for 1 hour, after which they were incubated with primary antibodies overnight at 4°C. The following day, the sections were washed 3 times with PBS; they were then incubated with fluorescently tagged secondary antibodies for 2 hours at RT in the dark. Finally, the sections were washed 3 times with TBS (adding DAPI into the last wash) and mounted onto glass slides using Mowiol 4-88 (Sigma-Aldrich). The sections were imaged using a CTR6500 confocal microscope equipped with Leica LAS AF software (Leica). Bielschowsky's staining was performed using the Bielschowsky Optim-Stain Kit as described (Hitobiotec Corp.) (57).

Lentiviruses and constructs. The human *ATXN1* coding sequence containing either 2 or 82 CAG repeats was subcloned from the FLAG-tagged pCDNA-ATXN1 construct into the pLEX lentiviral vector using SpeI and NotI as restriction sites (58). All lentiviruses were produced as mentioned previously (59). In brief, HEK293T cells were grown in DMEM High Glucose Medium (Gibco, Thermo Fisher Scientific) supplemented with 10% FBS, 2 mM L-glutamine, 100 U/ml penicillin, and 100 μg/ml streptomycin. At 80% confluency, cells were transfected with the lentiviral constructs along with the packaging vectors pCMV-VSV-G and pCMV Gag/pol using Lipofectamine 2000 reagent (Life Technologies/Thermo Fisher Scientific). After 48 to 72 hours, the supernatants containing virus particles were collected and filtered through a 0.45 μm filter. Viral particles were then concentrated using

Lenti-X Concentrator (Clontech). The relative infectivity was determined by a serial dilution of the virus. Single-cell neurosphere cultures were transduced with viruses on day 1 in vitro (DIV1), and experiments were conducted on day 8. The viral transduction efficiency of neurospheres was determined by quantifying the GFP-positive cells.

Antibodies. The following primary antibodies were used: mouse anti–prominin-1 (catalog 14-1331, clone 13A4; Affymetrix eBioscience), anti-rabbit nestin (catalog ab27952, Abcam), rabbit anti–β-tubulin III (catalog T2200, Sigma-Aldrich), mouse anti-tubulin, β III (MAB1637, Millipore), mouse anti-neurofilament H & M (NF-H/NF-M), mouse anti-phosphorylated neurofilament H & M (pNF-H/pNF-M) (catalog 801603, clone SMI 31, BioLegend), rabbit anti–PAX-2 (catalog 71-6000, Invitrogen), rabbit anti-vGAT (catalog 131 003, Synaptic systems-SY SY), rabbit anti-Nfasc (catalog ab31457, Abcam), mouse anti-GAD67 (catalog ab26116, Abcam), rabbit anti-Ki67 (catalog ab15580, Abcam), rabbit anti-GFAP (catalog Z0334, Dako), mouse anti-GAPDH (catalog 14C10, Cell Signaling Technology), mouse anti–β-actin (catalog A5316, Sigma-Aldrich), mouse anti-ATXN1 (11NQ clone N76/3; NeuroMab), mouse anti-GFAP (catalog MCA-5C10, Encor Biotechnology), and rabbit anti-HCN1 (gift of Dane M. Chetkovich, Northwestern University).

Quantitative analysis of basket score in human brain samples. Arnulf H. Koeppen (Albany Medical College, Albany, New York, USA) provided brain samples derived from autopsies of 12 genetically confirmed cases of SCA1 (Supplemental Table 1). All SCA1 brain samples were fixed in ice-cold 4% neutral formaldehyde solution as soon as harvested and embedded in paraffin. Autopsies were performed through a national tissue donation program supported by the National Ataxia Foundation.

The sectioning and staining of human samples was carried out at the Northwestern University Pathology Core Facility. Sections that were 5 μm thick were cut from each paraffin block and stained with pNfl (1:100) or Nfasc (1:70) antibody. Cerebellar sections were imaged at the Northwestern University Center for Advanced Microscopy using a Zeiss Axioscope Kit with CRi Naunce Spectral Camera (×20 objective lens). BC axonal processes were quantified in a blinded fashion. Basket processes surrounding each visible PC soma were traced using Adobe Photoshop (around 100 baskets/brain). The original digital images of BC tracings were inverted using ImageJ software (NIH) and converted into 9-bit gray scale. The integrated density of BC areas was then measured (each pixel of basket tracing was assigned a gray value using a variable gray scale and then summed) and the relative values categorized into 3 different scores: low, 0–3; moderate, 3–6; and high, 6–9 (31).

EM. Mice were perfused with EM grade 4% PFA. Cerebellar samples were isolated and embedded in OCT compound (13), and 150 μm–thick sagittal sections were cut using a vibratome (Leica). The sections were post-fixed in 2% PFA and 2.5% glutaraldehyde in 0.1 M sodium cacodylate buffer (pH 7.3) and incubated with unbuffered 2% osmium tetroxide. After rinsing with water, sections were stained with 3% uranyl acetate, followed by a rinse with water and subsequent dehydration in ethanol of ascending grades (50%, 70%, 80%, 90%, 100%). Sections were then embedded in resin mixture with Embed 812 and cured in a 60°C oven for 3 days. Sections in which the PC layer and molecular layer were visible under bright-field illumination on a dissection scope were selected. Approximately 5 mm wide × 7 mm long pieces of cerebellar cortex from these sections were dissected under the microscope, mounted on resin blocks, and sectioned on a Leica Ultracut UC6 Ultramicrotome. Sections 1 mm thick were collected and stained with Toluidine blue O (Sigma-Aldrich). Subsequently, 70 nm–thick sections were collected on Formvar carbon film (Agar Scientific) on slotted grids and stained with uranyl acetate and Reynolds lead citrate. Samples were processed and imaged at the Center of Advanced Microscopy at Northwestern University Feinberg School of Medicine (59).

Electrophysiology. Cerebellar brain slices were obtained from 20- to 37-day-old WT and SCA1-knockin mice that were anesthetized with isoflurane and euthanized by decapitation. The brains were quickly removed from the skull in warm temperature (30–33°C) and put into low Ca^{2+} and high Mg^{2+} artificial cerebrospinal fluid (ACSF) containing 87 mM NaCl, 25 mM $NaHCO_3$, 2.5 mM KCl, 1.25 mM NaH_2PO_4, 0.5 mM $CaCl_2$, 7 mM $MgCl_2$, 75 mM sucrose, and 25 mM glucose, bubbled with 95% O_2 and 5% CO_2 (pH 7.4). Sagittal cerebellar slices of 300 μm thickness were cut using a vibratome (Leica VT1200) and then stored in a solution containing 87 mM NaCl, 25 mM $NaHCO_3$, 2.5 mM KCl, 1.25 mM NaH_2PO_4, 0.5 mM $CaCl_2$, 7 mM $MgCl_2$, 75 mM sucrose, and 25 mM glucose, bubbled with 95% O_2 and 5% CO_2 (pH 7.4) for 15 minutes at 34°C and then at RT. For the recordings, slices were transferred to a recording chamber bathed in physiological ACSF (125 mM NaCl, 25 mM $NaHCO_3$, 2.5 mM KCl, 1.25 mM NaH_2PO_3, 25 mM glucose, 2.0 mM $CaCl_2$, and 1 mM $MgCl_2$, equilibrated with 95% O_2 and 5% CO_2) at 30–32°C. Slices were visualized using an upright microscope (Scientifica) with an Olympus ×60 water-immersion objective and infrared illumination.

Pipettes were pulled from borosilicate glass using a horizontal puller (P97, Sutter). Tip resistances ranged from 3 to 6 MΩ, yielding series resistances of 10 to 30 MΩ. Pipettes were filled with a CsCl-based internal solution consisting of 138 mM CsCl, 2 mM NaCl, 2 mM $MgCl_2$, 10 mM EGTA, 10 mM HEPES, 2 mM Na_2ATP, 0.03 mM NaGTP, pH 7.3 with CsOH; by blocking voltage-gated and leakage potassium currents, this solution allowed better clamp conditions for whole-cell recordings. Electrophysiological data were obtained using an Axopatch 200B amplifier and acquired and processed using Axion pClamp9 software. The membrane potential values are reported without correcting for liquid junction potentials. To study spontaneous inhibitory postsynaptic currents (sIPSC), fast glutamatergic transmission was blocked by adding 3 mM kynurenic acid. sIPSC recordings were performed at a holding potential of –80 mV so that inhibitory currents were inward, as the reversal potential for chloride is approximately 0 mV. Picrotoxin (100 μM) was bath applied to a number of cells to confirm that the spontaneous currents were $GABA_A$-R mediated. Recordings of 300 seconds duration were analyzed with Mini Analysis (Synaptosoft) and manually inspected to reject erroneous detection.

Microscopy and image analyses. Nikon Eclipse TE2000-E (Nikon Inc.) and Lieca TCS SP5 confocal microscopes (Leica Inc.) were used to acquire low- and high-magnification images of fluorescent samples, respectively. *Z*-stacks were processed using ImageJ. Light images were acquired using a Ds-Fil camera (Nikon). For EM imaging, grids were examined on an FEI Tecnai Spirit Transmission Electron Microscope at 120 kV using an FEI Eagle camera.

Statistics. GraphPad (Prism 4.0, GraphPad Software) was used to perform statistical tests and plot results. Data are presented as mean ± SEM. The level of significance was set at a P value of less than 0.05. Two-tailed t tests were used for comparison of the 2 data sets, while 2-way ANOVA followed by Bonferroni's correction was used for experiments with 3 or more data sets. Molecular and biochemical analyses were performed using a minimum of 3 biological replicates per condition.

Study approval. All animal experiments were performed in compliance with the NIH's *Guide for the Care and Use of Laboratory Animals* (National Academies Press, 2011) and were reviewed and approved by the Northwestern University IACUC (protocol IS00002501). A.H. Koeppen's research is approved by the Institutional Review Board of the Veterans Affairs Medical Center, Albany, New York, USA.

Author contributions

CRE and PO designed and conceptualized the study. CRE developed methods and performed all experiments except electrophysiology. JD and MM performed and analyzed electrophysiology experiments. AD prepared ATXN1 lentiviral constructs. CRE, JD, PO, and MM curated data. CRE wrote the original draft. CRE, PO, and AD wrote and reviewed and edited the manuscript. PO and MM provided resources. PO and MM acquired funding.

Acknowledgments

We thank members of the Opal lab for their suggestions, Vicky Brandt for thoughtful comments on the manuscript, James Scott Coy-Dibley for help with mouse genotyping, and Arnulf H. Koeppen, who provided SCA-1 brain material. Autopsies were performed through a national tissue donation program supported by the National Ataxia Foundation. PO is supported by NIH grants 1R01 NS062051 and 1R01 NS082351. MM is supported by NIH grant 1R21NS090346.

Address correspondence to: Puneet Opal, Davee Department of Neurology, and Department of Cell and Molecular Biology, Northwestern University Feinberg School of Medicine, Ward 10-332, 303 East Chicago Avenue, Chicago, Illinois 60611, USA. Phone: 312.503.4699; Email: P-opal@northwestern.edu.

1. Banfi S, et al. Identification and characterization of the gene causing type 1 spinocerebellar ataxia. *Nat Genet*. 1994;7(4):513–520.
2. Guo L, et al. A cellular system that degrades misfolded proteins and protects against neurodegeneration. *Mol Cell*. 2014;55(1):15–30.
3. Servadio A, Koshy B, Armstrong D, Antalffy B, Orr HT, Zoghbi HY. Expression analysis of the ataxin-1 protein in tissues from normal and spinocerebellar ataxia type 1 individuals. *Nat Genet*. 1995;10(1):94–98.
4. Watase K, et al. A long CAG repeat in the mouse Sca1 locus replicates SCA1 features and reveals the impact of protein solubility on selective neurodegeneration. *Neuron*. 2002;34(6):905–919.
5. Seidel K, Siswanto S, Brunt ER, den Dunnen W, Korf HW, Rüb U. Brain pathology of spinocerebellar ataxias. *Acta Neuropathol*. 2012;124(1):1–21.
6. Barnes JA, et al. Abnormalities in the climbing fiber-Purkinje cell circuitry contribute to neuronal dysfunction in ATXN1[82Q] mice. *J Neurosci*. 2011;31(36):12778–12789.
7. Ebner BA, et al. Purkinje cell ataxin-1 modulates climbing fiber synaptic input in developing and adult mouse cerebellum. *J Neurosci*. 2013;33(13):5806–5820.
8. Ruegsegger C, et al. Impaired mTORC1-dependent expression of Homer-3 influences SCA1 pathophysiology. *Neuron*. 2016;89(1):129–146.
9. Lin X, Antalffy B, Kang D, Orr HT, Zoghbi HY. Polyglutamine expansion down-regulates specific neuronal genes before pathologic changes in SCA1. *Nat Neurosci*. 2000;3(2):157–163.
10. Serra HG, Byam CE, Lande JD, Tousey SK, Zoghbi HY, Orr HT. Gene profiling links SCA1 pathophysiology to glutamate signaling in Purkinje cells of transgenic mice. *Hum Mol Genet*. 2004;13(20):2535–2543.
11. Ingram M, et al. Cerebellar transcriptome profiles of ATXN1 transgenic mice teveal SCA1 disease progression and protection pathways. *Neuron*. 2016;89(6):1194–1207.
12. Sánchez I, Balagué E, Matilla-Dueñas A. Ataxin-1 regulates the cerebellar bioenergetics proteome through the GSK3β-mTOR pathway which is altered in Spinocerebellar ataxia type 1 (SCA1). *Hum Mol Genet*. 2016;25(18):4021–4040.
13. Cvetanovic M, Patel JM, Marti HH, Kini AR, Opal P. Vascular endothelial growth factor ameliorates the ataxic phenotype in a mouse model of spinocerebellar ataxia type 1. *Nat Med*. 2011;17(11):1445–1447.
14. Cvetanovic M, Hu YS, Opal P. Mutant Ataxin-1 inhibits neural progenitor cell proliferation in SCA1. *Cerebellum*. 2017;16(2):340–347.
15. Asher M, Johnson A, Zecevic B, Pease D, Cvetanovic M. Ataxin-1 regulates proliferation of hippocampal neural precursors. *Neuroscience*. 2016;322:54–65.
16. Lee A, et al. Isolation of neural stem cells from the postnatal cerebellum. *Nat Neurosci*. 2005;8(6):723–729.
17. Fleming JT, et al. The Purkinje neuron acts as a central regulator of spatially and functionally distinct cerebellar precursors. *Dev Cell*. 2013;27(3):278–292.
18. Silbereis J, Cheng E, Ganat YM, Ment LR, Vaccarino FM. Precursors with glial fibrillary acidic protein promoter activity transiently generate GABA interneurons in the postnatal cerebellum. *Stem Cells*. 2009;27(5):1152–1163.
19. Parmigiani E, et al. Heterogeneity and bipotency of astroglial-like cerebellar progenitors along the interneuron and glial lineages. *J Neurosci*. 2015;35(19):7388–7402.
20. Goldfarb LG, et al. Unstable triplet repeat and phenotypic variability of spinocerebellar ataxia type 1. *Ann Neurol*. 1996;39(4):500–506.
21. Quan F, Janas J, Popovich BW. A novel CAG repeat configuration in the SCA1 gene: implications for the molecular diagnostics of spinocerebellar ataxia type 1. *Hum Mol Genet*. 1995;4(12):2411–2413.
22. Lim J, et al. Opposing effects of polyglutamine expansion on native protein complexes contribute to SCA1. *Nature*. 2008;452(7188):713–718.
23. Venkatraman A, et al. The histone deacetylase HDAC3 is essential for Purkinje cell function, potentially complicating the use of HDAC inhibitors in SCA1. *Hum Mol Genet*. 2014;23(14):3733–3745.
24. Bowman AB, et al. Duplication of Atxn1l suppresses SCA1 neuropathology by decreasing incorporation of polyglutamine-expanded ataxin-1 into native complexes. *Nat Genet*. 2007;39(3):373–379.
25. Crespo-Barreto J, Fryer JD, Shaw CA, Orr HT, Zoghbi HY. Partial loss of ataxin-1 function contributes to transcriptional dysregulation in spinocerebellar ataxia type 1 pathogenesis. *PLoS Genet*. 2010;6(7):e1001021.
26. Buttermore ED, Piochon C, Wallace ML, Philpot BD, Hansel C, Bhat MA. Pinceau organization in the cerebellum requires distinct functions of neurofascin in Purkinje and basket neurons during postnatal development. *J Neurosci*. 2012;32(14):4724–4742.
27. Ango F, di Cristo G, Higashiyama H, Bennett V, Wu P, Huang ZJ. Ankyrin-based subcellular gradient of neurofascin, an immunoglobulin family protein, directs GABAergic innervation at purkinje axon initial segment. *Cell*. 2004;119(2):257–272.
28. He Q, et al. Interneuron- and GABA(A) receptor-specific inhibitory synaptic plasticity in cerebellar Purkinje cells. *Nat Commun*. 2015;6:7364.
29. Kim J, et al. Optogenetic mapping of cerebellar inhibitory circuitry reveals spatially biased coordination of interneurons via electrical synapses. *Cell Rep*. 2014;7(5):1601–1613.
30. Blot A, Barbour B. Ultra-rapid axon-axon ephaptic inhibition of cerebellar Purkinje cells by the pinceau. *Nat Neurosci*. 2014;17(2):289–295.
31. Erickson-Davis CR, Faust PL, Vonsattel JP, Gupta S, Honig LS, Louis ED. "Hairy baskets" associated with degenerative Purkinje cell changes in essential tremor. *J Neuropathol Exp Neurol*. 2010;69(3):262–271.
32. Luján R, Albasanz JL, Shigemoto R, Juiz JM. Preferential localization of the hyperpolarization-activated cyclic nucleotide-gated cation channel subunit HCN1 in basket cell terminals of the rat cerebellum. *Eur J Neurosci*. 2005;21(8):2073–2082.
33. Everett CM, Wood NW. Trinucleotide repeats and neurodegenerative disease. *Brain*. 2004;127(11):2385–2405.
34. Jacobi H, et al. The natural history of spinocerebellar ataxia type 1, 2, 3, and 6: a 2-year follow-up study. *Neurology*. 2011;77(11):1035–1041.
35. Jacobi H, et al. Biological and clinical characteristics of individuals at risk for spinocerebellar ataxia types 1, 2, 3, and 6 in the longitudinal RISCA study: analysis of baseline data. *Lancet Neurol*. 2013;12(7):650–658.
36. Tezenas du Montcel S, et al. Prediction of the age

at onset in spinocerebellar ataxia type 1, 2, 3 and 6. *J Med Genet*. 2014;51(7):479–486.
37. Li P, et al. A population of Nestin-expressing progenitors in the cerebellum exhibits increased tumorigenicity. *Nat Neurosci*. 2013;16(12):1737–1744.
38. Clark HB, et al. Purkinje cell expression of a mutant allele of SCA1 in transgenic mice leads to disparate effects on motor behaviors, followed by a progressive cerebellar dysfunction and histological alterations. *J Neurosci*. 1997;17(19):7385–7395.
39. Cvetanovic M, Ingram M, Orr H, Opal P. Early activation of microglia and astrocytes in mouse models of spinocerebellar ataxia type 1. *Neuroscience*. 2015;289:289–299.
40. Iwakura A, Uchigashima M, Miyazaki T, Yamasaki M, Watanabe M. Lack of molecular-anatomical evidence for GABAergic influence on axon initial segment of cerebellar Purkinje cells by the pinceau formation. *J Neurosci*. 2012;32(27):9438–9448.
41. Pouzat C, Hestrin S. Developmental regulation of basket/stellate cell-->Purkinje cell synapses in the cerebellum. *J Neurosci*. 1997;17(23):9104–9112.
42. Ichikawa R, et al. Developmental switching of perisomatic innervation from climbing fibers to basket cell fibers in cerebellar Purkinje cells. *J Neurosci*. 2011;31(47):16916–16927.
43. Kuo SH, et al. Lingo-1 expression is increased in essential tremor cerebellum and is present in the basket cell pinceau. *Acta Neuropathol*. 2013;125(6):879–889.
44. Herson PS, et al. A mouse model of episodic ataxia type-1. *Nat Neurosci*. 2003;6(4):378–383.
45. Grimaldi P, Parras C, Guillemot F, Rossi F, Wassef M. Origins and control of the differentiation of inhibitory interneurons and glia in the cerebellum. *Dev Biol*. 2009;328(2):422–433.
46. Sudarov A, Turnbull RK, Kim EJ, Lebel-Potter M, Guillemot F, Joyner AL. Ascl1 genetics reveals insights into cerebellum local circuit assembly. *J Neurosci*. 2011;31(30):11055–11069.
47. Delaney CL, Brenner M, Messing A. Conditional ablation of cerebellar astrocytes in postnatal transgenic mice. *J Neurosci*. 1996;16(21):6908–6918.
48. Tao J, et al. Deletion of astroglial Dicer causes non-cell-autonomous neuronal dysfunction and degeneration. *J Neurosci*. 2011;31(22):8306–8319.
49. Cui W, Allen ND, Skynner M, Gusterson B, Clark AJ. Inducible ablation of astrocytes shows that these cells are required for neuronal survival in the adult brain. *Glia*. 2001;34(4):272–282.
50. Albanito L, Reddy CE, Musti AM. c-Jun is essential for the induction of Il-1β gene expression in in vitro activated Bergmann glial cells. *Glia*. 2011;59(12):1879–1890.
51. Farmer WT, et al. Neurons diversify astrocytes in the adult brain through sonic hedgehog signaling. *Science*. 2016;351(6275):849–854.
52. Kenney AM, Segal RA. Subtracting the math: prominin-positive cerebellar stem cells in white matter. *Nat Neurosci*. 2005;8(6):699–701.
53. Kriegstein A, Alvarez-Buylla A. The glial nature of embryonic and adult neural stem cells. *Annu Rev Neurosci*. 2009;32:149–184.
54. Matilla A, et al. Mice lacking ataxin-1 display learning deficits and decreased hippocampal paired-pulse facilitation. *J Neurosci*. 1998;18(14):5508–5516.
55. Reddy CE, et al. Multisite phosphorylation of c-Jun at threonine 91/93/95 triggers the onset of c-Jun pro-apoptotic activity in cerebellar granule neurons. *Cell Death Dis*. 2013;4:e852.
56. Schildge S, Bohrer C, Beck K, Schachtrup C. Isolation and culture of mouse cortical astrocytes. *J Vis Exp*. 2013;(71):50079.
57. Makar TK, et al. Silencing of Abcc8 or inhibition of newly upregulated Sur1-Trpm4 reduce inflammation and disease progression in experimental autoimmune encephalomyelitis. *J Neuroinflammation*. 2015;12:210.
58. Emamian ES, et al. Serine 776 of ataxin-1 is critical for polyglutamine-induced disease in SCA1 transgenic mice. *Neuron*. 2003;38(3):375–387.
59. Israeli E, et al. Intermediate filament aggregates cause mitochondrial dysmotility and increase energy demands in giant axonal neuropathy. *Hum Mol Genet*. 2016;25(11):2143–2157.